Journal of Materials Chemistry B

ROYAL SOCIETY OF CHEMISTRY

PAPER

View Article Online
View Journal | View Issue

Cite this: J. Mater. Chem. B, 2024, 12, 2618

Microneedle-assisted percutaneous delivery of methotrexate-loaded nanoparticles enabling sustained anti-inflammatory effects in psoriasis therapy†

Hongyao Du,‡[a] Jing Yang,‡[a] Mo Li,[b] Yuting Xia,[a] Yan Li,[a] Jintao Zhu,[b] Lianbin Zhang *[b] and Juan Tao *[a]

Received 7th November 2023,
Accepted 8th February 2024

DOI: 10.1039/d3tb02643d

rsc.li/materials-b

Methotrexate (MTX) is one of the first-line drugs used for the treatment of moderate to severe psoriasis. However, low bioavailability and systemic side effects of traditional oral and injectable MTX greatly limit its clinical application. Delivering MTX using dissolving microneedles (MNs) into psoriasis-like skin lesion could improve the *in situ* therapeutic effects with higher bioavailability and less side effects. Here, we propose a novel therapeutic approach for psoriasis involving MN-assisted percutaneous delivery of chitosan-coated hollow mesoporous silica nanoparticles containing MTX (MTX@HMSN/CS). The MTX@HMSN/CS-loaded MNs were strong enough to successfully penetrate the psoriasiform thickened epidermis, allowing MTX@HMSN/CS to be accurately delivered to the site of skin lesion following the rapid dissolution of MNs. MTX was then released continuously from HMSN/CS for at least one week to maintain effective therapeutic drug concentration for skin lesion with long-term anti-proliferative and anti-inflammatory effects. Incubation with MTX@HMSN/CS not only inhibited the proliferation of human immortalized keratinocytes (HaCaT cells), but also significantly reduced the expression of proinflammatory cytokines and chemokines. In addition, MTX@HMSN/CS-loaded MNs showed better efficacy in alleviating psoriasis-like skin inflammation than MTX-loaded MNs at the same dose. Compared to psoriasiform mice treated with 15.8 μg MTX-loaded MNs every day, 47.4 μg MTX@HMSN/CS-loaded MNs reduce the frequency of treatment to once every 3 days and achieve comparable amelioration. Therefore, MTX@HMSN/CS loaded MNs are a promising treatment strategy for psoriasis due to their durability, efficacy, convenience, and safety in relieving psoriasis-like skin inflammation.

1. Introduction

Psoriasis is a chronic inflammatory skin disease that is prone to relapse and severely impairs the life quality of patients.[1,2] Methotrexate (MTX) is an immunosuppressant and metabolite widely used in the treatment of moderate to severe psoriasis.[3–5] For many years, MTX has been administered orally and by injection. Although effective, there are still some adverse effects that hinder its widespread application.[6,7] Oral administration can cause gastrointestinal side effects such as nausea, vomiting, diarrhea, and abdominal pain.[8,9] First-pass elimination also reduces the bioavailability of MTX. Injections can cause pain and bleeding.[10,11] Both high dose injection and oral MTX have the risk of liver and kidney damage, bone marrow suppression and infection.[12,13] Therefore, there is an urgent need to develop safer and more effective MTX delivery methods.

In recent years, microneedle (MN) technology has attracted plenty of attention in the field of transdermal drug delivery.[14–17] It has developed into one of the most effective methods of promoting the transdermal delivery of cells, macromolecular drugs and antigens.[18–20] Local administration of MNs can effectively penetrate the stratum corneum of the skin without touching nerves, avoiding pain and gastrointestinal discomfort, while increasing the bioavailability of drug.[21–23] In addition, MN transdermal drug delivery operation is simple and allows patients to use it alone without professional training.[24–26] Dissolving MNs are made from water-soluble polymers that dissolve and release drugs into the skin. They have the advantages of facile preparation, high drug load and high safety, and has excellent application prospects.[27–29] In our

[a] Hubei Engineering Research Center for Skin Repair and Theranostics, Department of Dermatology, Union Hospital, Tongji Medical College, Huazhong University of Science and Technology (HUST), Wuhan 430022, China. E-mail: tjhappy@126.com

[b] Key Laboratory of Material Chemistry for Energy Conversion and Storage (HUST), Ministry of Education, School of Chemistry and Chemical Engineering, HUST, Wuhan 430074, China. E-mail: zhanglianbin@hust.edu.cn

† Electronic supplementary information (ESI) available. See DOI: https://doi.org/10.1039/d3tb02643d

‡ These authors contributed equally to this work.

previous study, we treated psoriasis directly by loading MTX into dissolved hyaluronic acid MNs. The MTX-loaded MNs successfully penetrate the thickened skin and deliver drugs into the skin, successfully reducing the inflammatory response to mouse skin lesions in mice.[30] However, such MNs rapidly dissolve in local skin. The rapid release of MTX resulted in the high uptake of drug into the blood vessels, reducing the drug utilization rate. As a result, it is difficult to maintain the required concentration of therapeutic agents in the skin just by dissolving MNs. Further improvements are highly desired in MTX-loaded MNs to improve their therapeutic effect.

Nanocarriers are attracting growing interest because they prevent drug degradation or inactivation and extend the life of drugs to improve their bioavailability and therapeutic efficacy.[31–33] There are increasing efforts to combine nanocarriers and dissolving MNs as alternatives to current constraints.[34–36] Donnelly *et al.* successfully encapsulated MTX into nanocrystal-loaded MN arrays and achieved continuous drug release for 72 hours.[37] But the efficacy of the MN array was not studied in psoriasis animal models. Chen *et al.* recently developed an MN patch that localizes MTX-loaded human serum albumin nanoparticles (NPs) to lymph nodes to improve the antipsoriatic effect.[38] Nonetheless, the *in vivo* efficacy of MTX-loaded MNs drug delivery systems also needed further exploration.

To break the limitations of conventional systemic administration of MTX, we combined hybrid drug-loaded NPs with dissolving MNs to achieve a sustained-release system for transdermal MTX delivery, utilizing controlled release of nanocarriers to significantly slow down drug release. First, we synthesized hollow mesoporous silica nanoparticles (HMSN) and encapsulated MTX into the cavity of HMSN by a solvent evaporation method. Then, we used electrostatic interactions to adsorb positively charged chitosan (CS) to the surface of HMSN and obtained chitosan-coated hollow mesoporous silica nanoparticles loaded with MTX (MTX@HMSN/CS). Nanocarriers were able to release the drug *in vitro* for up to seven days in a sustained manner and could effectively inhibit the proliferation of human immortalized keratinocytes (HaCaT cells). We used the microtemplating method to load MTX@HMSN/CS into a dissolving MN patch and used it to treat a psoriasis-like mouse model. The anti-inflammatory effect of transdermal delivery of MTX by MN patches was significantly enhanced as MTX@HMSN/CS could release MTX slowly after being delivered into the local skin *via* MNs, thus avoiding rapid drug diffusion and uptake in blood vessels. The combination of hybrid drug-loaded NPs and MNs dramatically improves drug availability and frequency of treatment, providing a novel approach for sustained anti-inflammatory treatment of psoriasis.

2. Experimental

2.1. Materials

Cetyltrimethylammonium bromide (CTAB) and polyvinyl alcohol (PVA) were acquired from Sigma-Aldrich (St. Louis, MO, USA). Chitosan (CS) and polyvinylpyrrolidone (PVP) were supplied by Aladdin Reagent Co.; Ltd (Shanghai, China). Tetraethyl orthosilicate (TEOS) was purchased from China National Pharmaceutical Group Corporation (Shanghai, China). Chondroitin sulfate (ChS) was bought from Meilun Biotechnology Co.; Ltd (Dalian, China). Methotrexate (MTX) was obtained from Adamas Reagent, Ltd (Basel, Switzerland). Imiquimod (IMQ) cream 5% was supplied by Mingxin Pharmaceuticals (Sichuan, China). The Sylgard® 184 silicone elastomer kit was provided by Dow Corning Krayden Inc. (Midland, Michigan, USA). All other chemicals and reagents were of analytical/pharmaceutical grade and used without further purification.

2.2. Animals

BALB/c mice (8–10 weeks old, 18–20 g) employed in this study were purchased from Beijing Huafukang Biological Technology Co.; Ltd (Beijing, China). Mice were housed under specific pathogen-free conditions at 22–24 °C with a 12-h light/dark cycle and unlimited access to food and water. All animal experiments were performed in accordance with ''The Guide for the Care and Use of Laboratory Animals of Huazhong University of Science and Technology'' and approved by the Institutional Animal Care and Use Committee, Tongji Medical College, Huazhong University of Science and Technology.

2.3. Preparation of MTX@HMSN/CS

HMSN were first synthesized according to our previous report and were dispersed in water and stored in a refrigerator at 4 °C.[39] MTX and HMSN were dispersed in DMSO at a specific ratio and stirred overnight. The DMSO was removed by negative pressure at a low temperature to encapsulate MTX into HMSN. The mixture was then washed with H_2O three times. Finally, MTX@HMSN were dispersed in a CS solution (0.6% wt) and stirred at 30 °C for 2 hours. CS was adsorbed to the surface of MTX@HMSN due to electrostatic interactions, and the obtained suspension was centrifuged and dried to obtain MTX@HMSN/CS (Fig. 1(a)).

2.4. Characterizations of HMSN, HMSN/CS and MTX@HMSN/CS

The HMSN, HMSN/CS and MTX@HMSN/CS were characterized by transmission electron microscope (TEM; Tecnai G220, FEI company, Holland), a surface area and porosity analyzer (TriStar II 3020, Micromeritics Instrument Corporation, United States), and a laser particle size analyzer (LB-550, HORIBA, Japan). The particle size and zeta potential of MTX@HMSN/CS and HMSN were measured by dynamic light scattering (DLS). The surface chemistry and structure of the HMSN were characterized by Fourier transform infrared (FTIR) spectroscopy (VERTEX 70, Bruker, Germany). Furthermore, the mass of CS coated on the surface of HMSN was quantitatively detected in an atmosphere of N_2 by thermogravimetric analysis (TGA). Drug loading capacity (DL) and encapsulation efficiency (EE) of MTX were determined using an ultraviolet-visible (UV-Vis) spectrophotometer (UV-1800, Shimadzu, Japan) at a detection wavelength of 372 nm (the characteristic wavelength of MTX).

The DL and EE were calculated using the equations given below:

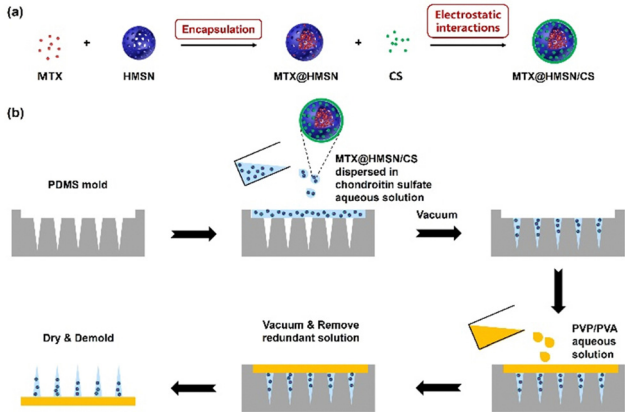

Fig. 1 Schematic illustration showing the preparation of the MTX@HMSN/CS-loaded MN patch. (a) Schematic diagram of the synthesis process of MTX@HMSN/CS. (b) Schematic diagram showing the two-step micromolding process during the fabrication of the MN patch.

$$\text{DL} = (\text{Mass of loaded drug}/\text{Mass of drug loaded nanocarriers}) \times 100\%$$

$$\text{EE} = (\text{Mass of loaded drug}/\text{Total dosage}) \times 100\%$$

2.5. *In vitro* release of MTX from MTX@HMSN/CS

MTX@HMSN and MTX@HMSN/CS were dispersed in PBS solution, respectively. Drug release from MTX@HMSN and MTX@HMSN/CS was measured in a shaking water bath (37 °C, 120 rpm). The sample suspension (1.0 mL each) was taken out at predetermined time points (0, 2, 4, 8, 12, 24, 48, 72, 96, 120, 144 and 168 h), and 1.0 mL of fresh PBS solution was added to ensure that the volume remained constant. We determined the absorbance of the supernatant by UV-Vis spectrophotometer at 372 nm. By comparing the absorbance of samples with the standard curve, the MTX concentration of the supernatant obtained at each time point of each group of samples and the accumulated release percentage of MTX were determined. The morphological changes of MTX@HMSN/CS were also observed by TEM.

2.6. Fabrication of MTX@HMSN/CS-loaded MN patches

The MTX@HMSN/CS-loaded MN patches were fabricated by a two-step micromolding process (Fig. 1(b)). We chose ChS, with good biocompatibility and solubility, as the matrix material of each needle of the MN patch. In brief, the MTX@HMSN/CS were dispersed in ChS aqueous solution (200 mg mL^{-1}) to obtain the matrix suspension of needles. Then, 300 mg of PVA powder and 300 mg of PVP powder were dissolved in 2 mL of deionized water to obtain the matrix solution of the substrate of the MN patch. The polydimethylsiloxane (PDMS) molds were first filled with the matrix suspension of needles, followed by vacuum treatment (~0.08 MPa) in a vacuum oven. The excess suspension was scraped away from the surface of the mold. Then, the samples were dried in a sealed desiccator overnight at room temperature. A layer of the matrix solution of substrates was poured over the samples. Subsequently, we put these samples into a vacuum oven to make the basal layer adhere to the needle. After being peeled off from the molds, all the final MTX@HMSN/CS-loaded MN patches were sealed and stored in desiccators at room temperature.

2.7. Morphology, drug loading and mechanical properties of MTX@HMSN/CS-loaded MNs

The MN patches were observed and photographed using a dermoscope. The needles of the MTX@HMSN/CS-loaded MN patches were carefully collected and dissolved in sodium hydroxide solution and ultrasonicated to release the drug completely. The absorbance at 372 nm wavelength of the solution was detected using an UV-Vis spectrophotometer to calculate the drug loading. The mechanical strength of the MN patches loaded with different concentrations of MTX@HMSN/CS was evaluated using a universal texture tensile testing machine (CMT4202, Xinsansi, China) with the compression mode. The shape changes of the MNs when they were compressed were observed and recorded using a dermoscope.

2.8. *In vivo* skin insertion experiments of MTX@HMSN/CS-loaded MNs

2.8.1. *In vivo* skin insertion capability and acute skin irritation test of MTX@HMSN/CS-loaded MNs. The skin insertion capability of MTX@HMSN/CS-loaded MNs was tested with IMQ-induced psoriasis-like mouse ear skin lesion. We applied approximately 20 mg of IMQ cream to a mouse's left ear for 6 days, and the psoriasis animal model was established on the seventh day. After 5-min treatment with the MTX@HMSN/CS-loaded MN patch, the MN-pierced skin was cut off, fixed with 4% paraformaldehyde and embedded in paraffin. For histological observation, skin tissue sections of 4 μm thickness were stained with H&E. The samples were observed using an optical microscope (IX71, Olympus, Tokyo, Japan).

The acute skin irritation test of MTX@HMSN/CS-loaded MNs was also conducted *in vivo*. Photographs were taken pretreatment and at 0, 3, 10, 20, 30, 45 and 60 min after treatment using a dermoscope. The animals were anesthetized by intraperitoneal injection of pentobarbital sodium.

2.8.2. *In vivo* dissolution of MTX@HMSN/CS-loaded MNs. For *in vivo* dissolution analysis of the MTX@HMSN/CS-loaded MNs, the hair on the back of mice was removed before insertion. The MNs were taken off from the skin at different time intervals (3, 5 and 10 min) and then observed from a side view using an optical microscope (IX71, Olympus, Tokyo, Japan). Furthermore, MTX@HMSN/CS-loaded MN patches were observed using a scanning electron microscope (SEM; Nova NanoSEM 450, FEI, Eindhoven, The Netherlands) before and after dissolution in skin.

2.9. Drug permeation study of MTX@HMSN/CS-loaded MNs

In order to observe drug permeation into skin, MTX was replaced by dye rhodamine 6G (R6G) during the production process of MNs. The *in vitro* skin penetration performance of R6G@HMSN/CS-loaded MNs were observed using a confocal

laser scanning microscope (CLSM; FV1200, Olympus, Japan). R6G@HMSN/CS-loaded MNs were inserted into the fresh porcine skin for 5 minutes. The MN tips of the patches dissolved, and the dye-loaded HMSN/CS diffused into the skin. The fluorescence signal in the skin treated with the MN patches was observed using CLSM at an excitation wavelength of 526 nm. After the *xy* plane with the maximum and minimum fluorescence intensity was determined, images were obtained from the *xy*-plane at a scan interval of 10 μm in the *z*-axis to observe the dye diffusion in the skin.

2.10. *In vitro* cell experiments

An immortalized human keratinocyte cell line (HaCaT cell) bought from China Center for Type Culture Collection (CCTCC) was employed to test the *in vitro* antiproliferative and anti-inflammatory effects of MTX@HMSN/CS. A total of 1×10^4 HaCaT cells were seeded in each well of a 96-well plate and cultured in Dulbecco's modified Eagle's medium (DMEM; Gibco, USA) supplemented with 10% (v/v) fetal bovine serum (FBS; CellMax, China) and 1% (v/v) penicillin–streptomycin solution. The plate was incubated at 37 °C in 5% CO_2 for 24 hours to allow HaCaT cells to attach. Then, all culture medium was removed, and the plate was washed twice with PBS solution. We used IL-17A (100 ng mL^{-1}) to stimulate the proliferation of HaCaT cells. In addition, the cells in different groups were cultured in different media containing HMSN/CS or MTX@HMSN/CS at a series of concentrations. The cells cultured in a basic medium served as a control group. After 48 h of incubation, all culture medium was removed, and the plate was washed twice with PBS solution. Subsequently, 100 μL of fresh DMEM containing 10% (v/v) Cell Counting Kit-8 (CCK-8; Dojindo, Japan) was added to the plate. Finally, the absorbance of each well was measured at 450 nm using an ELISA microplate reader (TECAN Infinite F50, Switzerland) 2 h later to evaluate cell viability. We also determined the key proinflammatory cytokines (IL-1β, IL-6) and chemokines (CCL20) in the supernatants to evaluate the anti-inflammatory effects of MTX@HMSN/CS using ELISA kits.

2.11. *In vivo* study of the therapeutic and adverse effects

The therapeutic effects of the prepared MTX@HMSN/CS-loaded MN patches on psoriasis and their adverse effects were evaluated using a psoriasis-like mouse model. Female BALB/c mice were randomly divided into 8 groups (5 mice per group). The mice given no IMQ cream served as a control group (Control), while mice in the other 7 groups received topical application of IMQ cream (20 mg per day) for 9 consecutive days (day 1 to 9) on their left ears and were differently treated: (1) psoriasis model group (Model), (2) unloaded MN group (blank MN patch), (3) HMSN/CS-loaded MN group, (4) oral MTX group, (5) 47.4 μg MTX-loaded MN group, (6) 47.4 μg MTX@HMSN/CS-loaded MN group, and (7) 15.8 μg MTX-loaded MN group. MTX solution (~47.4 μg MTX) was orally administered to each mouse every 3 days in the oral MTX group. Mice in the unloaded MN group, HMSN/CS-loaded MN group, 47.4 μg MTX-loaded MN group, and 47.4 μg MTX@HMSN/CS-loaded MN group were treated with MNs every three days. But in the 15.8 μg MTX-loaded MN group, the mice were given daily MN treatment.

The severity of skin inflammation was assessed by daily measuring the ear thickness using a Vernier caliper. On day 10, ear lesions in all groups were observed and photographed. Before the mice were sacrificed, blood samples were collected to evaluate the function of the liver and kidney. Finally, the left ears of all mice were cut off, fixed with 4% paraformaldehyde, and embedded in paraffin, followed by H&E staining, immunohistochemical staining for Ki67, and immunofluorescence staining for CD3 and IL-17A. All stained slides were observed using an optical microscope or an inverted fluorescence microscope (IX71, Olympus, Tokyo, Japan). Representative microphotographs were taken, and the counts of $Ki67^+$ cells as well as $IL\text{-}17A^+$ T cells were quantitatively analyzed. Epidermal thickness was measured using ImageJ software (1.47v, National Institutes of Health, Bethesda, MD).

2.12. Statistical analysis

All experiments were conducted at least three times independently and repeated in triplicate. The original data were analyzed and calculated using GraphPad Prism software (v9.3.0). Data were presented as mean ± standard deviations ($n \geq 3$). The statistical differences between two groups were determined by unpaired Student's *t*-test. Multiple groups comparisons were evaluated by one-way ANOVA. The differences were deemed to be statistically significant when $^*p < 0.05$, $^{**}p < 0.01$, $^{***}p < 0.001$, and $^{****}p < 0.0001$ were observed, while ns (not significant) suggested that $p > 0.05$.

3. Results and discussion

3.1. Characterization of HMSN, HMSN/CS, and MTX@HMSN/CS

The TEM image of the obtained HMSN showed that they had a regular spherical shape with a diameter of 200–300 nm, and the shell thickness was approximately 40 nm (Fig. 2(a)). HMSN exhibited a typical hollow mesoporous structure, providing abundant drug-loading space. According to the N_2 isothermal adsorption–desorption curve of HMSN, the specific surface area of HMSN was 703.4 m^2 g^{-1}, and the pore volume was 0.59 cm^3 g^{-1} (Fig. 2(b)). The analysis of mesopore pore size distribution showed a mesopore pore size of approximately 2.5 nm (Fig. 2(c)). The results suggested that the mesopores on the surface of HMSN could be used to load and release drugs smoothly. Fig. 2(d) displays a TEM photo of MTX@HMSN/CS. There was a thin layer of CS on the surface of HMSN, and CS can block the mesopores on the surface of HMSN to prevent drug leakage. The particle size of MTX@HMSN/CS was 464.8 ± 45.31 nm, and the particle diameter of HMSN was 295.2 ± 66.36 nm (Fig. 2(e)). After CS was adsorbed on the surface of HMSN, the particle size increased significantly (Fig. S1, ESI†). The change in zeta potential further proved that CS was successfully adsorbed on the surface of HMSN. The

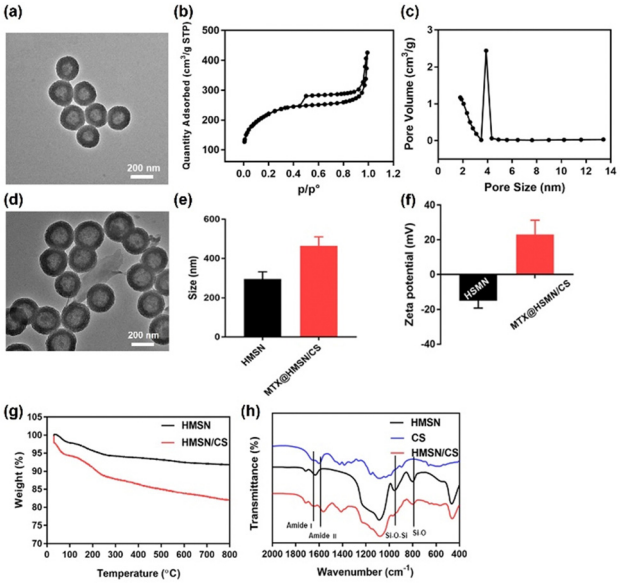

Fig. 2 Characterization of HMSN, HMSN/CS and MTX@HMSN/CS. (a) TEM image of HMSN. (b) N_2 isothermal adsorption–desorption curve of HMSN. (c) Pore size distribution analysis of HMSN. (d) TEM image of MTX@HMSN/CS. (e) Particle sizes of HMSN and MTX@HMSN/CS. (f) Zeta potentials of HMSN and MTX@HMSN/CS. (g) TGA curves of HMSN and HMSN/CS. (h) FTIR spectra of CS, HMSN and HMSN/CS.

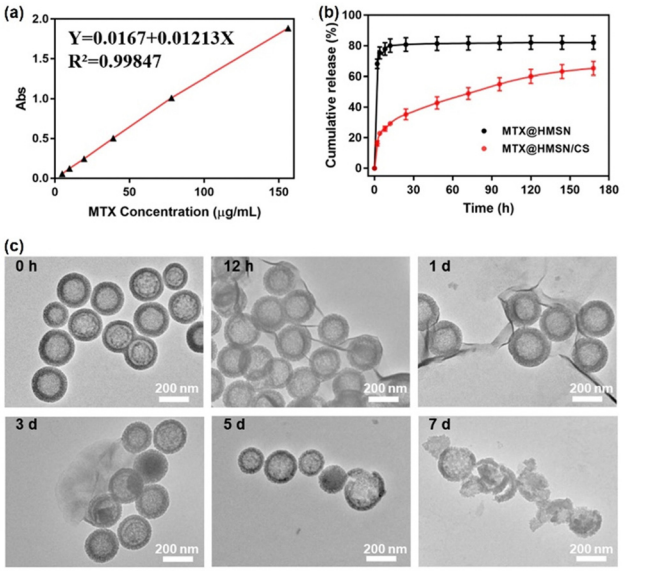

Fig. 3 *In vitro* release of MTX from MTX@HMSN/CS. (a) Absorbance standard curve of MTX. (b) *In vitro* release curve of MTX@HMSN and MTX@HMSN/CS. (c) Morphology changes of MTX@HMSN/CS during the drug release process *in vitro*.

surface zeta potential of HMSN in water was -14.9 ± 4.29 mV, and the zeta potential of MTX@HMSN/CS was reversed, indicating that the positively charged CS polymer molecules adsorbed on the surface of HMSN through electrostatic interactions (Fig. 2(f)). The content of the CS on the HMSN was evaluated by TGA. When the temperature increased to 800 °C, the weight loss of HMSN without CS coating reached 8.19%, and the weight loss reached 17.98% when CS was coated on the surface of HMSN by electrostatic interaction. The mass ratio of HMSN to CS in HMSN/CS was 10.7 : 1. These results indicated that CS was effectively adsorbed onto the surface of HMSN (Fig. 2(g)). The FTIR spectra of CS, HMSN, and HMSN/CS are shown in Fig. 2(h). Compared with HMSN, the appearance of the characteristic absorption peaks at 1664 cm^{-1} and 1565 cm^{-1} belonging to the amide I band and amide II band can be observed in the spectra of HMSN/CS, demonstrating the successful adsorption of CS on the surface of HMSN. The DL and EE values of MTX in HMSN/CS were calculated to be 23.75% ± 1.24% and 62.31% ± 4.27%, respectively.

3.2. *In vitro* release of MTX from MTX@HMSN/CS

The relationship equation between MTX concentration and absorbance is $Y = 0.0167 + 0.01213X$, and the correlation coefficient $R^2 = 0.99847$, which proves that there is a good linear relationship between MTX concentration and absorbance within the concentration range of 0 to 150 μg mL^{-1} (Fig. 3(a)). MTX was loaded into the cavity of HMSN by negative pressure and then HMSN was coated with CS. Fig. 3(b) shows the MTX release curves of MTX@HMSN/CS and MTX@HMSN in phosphate buffered saline (PBS) solution with pH = 7.4 at 37 °C, which imitated the *in vivo* conditions. MTX@HMSN without CS coating had a pronounced rapid drug release process. The cumulative release amount reached approximately 65% in the first two hours, and the release of MTX approached the maximum of 80% within 24 hours. The coating of CS blocked the pores of HMSN so that the drug would not be released quickly. The release curve of MTX@HMSN/CS showed that only about 18% of the drug was released within the first two hours since the drug adsorbed on the surface of MTX@HMSN/CS was the earliest to be released. The pores on the surface of HMSN were exposed with the dissociation of CS, and HMSN/CS also gradually degraded over time. Consequently, the drug loaded in HMSN/CS continued to be released over 7 days with a slower drug release rate. The release of MTX reached around 35%, 43%, 49%, 55%, 59%, 61% and 63% at 24 h, 48 h, 72 h, 96 h, 120 h, 144 h, and 168 h, respectively. We also characterized the morphology of MTX@HMSN/CS during the drug release process by TEM (Fig. 3(c)). At first, the CS on the surface of MTX@HMSN/CS gradually dissociated. Afterward, the degradation of MTX@HMSN/CS was observed in the field of view. Finally, over 80% of the HMSN were broken after 7 days. The results indicated that MTX@HMSN/CS achieved the sustained release of MTX through the dissociation of CS and the degradation of nanocarriers.

3.3. Morphology, drug loading and mechanical properties of MTX@HMSN/CS-loaded MNs

The MTX@HMSN/CS-loaded MN patches were fabricated by a two-step micromolding process, as described in the Experimental section. The dermoscope images of the unloaded MN patch and MTX@HMSN/CS-loaded MN patch showed that the array of MNs was 10 × 10, and the needle tip was in the shape

of a relatively regular quadrangular pyramid. The needle tip is sharp and clear, and the height of the needle is approximately 750 μm. The blank MNs appear transparent, while the MNs loaded with MTX@HMSN/CS appear pale yellow due to the presence of MTX (Fig. 4(a) and (b)). We found that the MN patch showed a larger loading capacity as the concentration of MTX@HMSN/CS increased (Fig. 4(c)). When the mass ratios of MTX@HMSN/CS to ChS were 1 : 5, 1 : 4, 1 : 3, and 1 : 2, the drug loadings of the MN patches were 28.87 ± 6.33 μg, 39.22 ± 7.34 μg, 57.13 ± 7.73 μg, and 85.99 ± 11.33 μg, respectively. These results indicated that we could adjust the amount of the drug loaded in the MN patches by changing the concentration of MTX@HMSN/CS in the matrix solution for precise therapy strategies. Furthermore, we also adjusted the mechanical strength of the MNs by changing the content of MTX@HMSN/CS in the MNs (Fig. 4(d)). The mechanical strength of the blank MN with no NPs was over 0.3 N per needle (Fig. 4(e)). When the mass ratios of MTX@HMSN/CS to ChS were 1 : 5, 1 : 4, 1 : 3, and 1 : 2, the force that each needle tip of the MNs could withstand was about 0.18 N, 0.1 N, 0.08 N, and 0.06 N, respectively (Fig. 4(f)). The mechanical strength of the MNs decreases along with the increase in the amount of MTX@HMSN/CS loaded in the MNs, indicating that the encapsulation of MTX@HMSN/CS into the MNs would reduce their mechanical strength. Finally, MNs became bent but did not break with the increase of force, suggesting that needles of MN patches prepared from ChS had excellent strength and toughness (Fig. 4(g) and (h)).

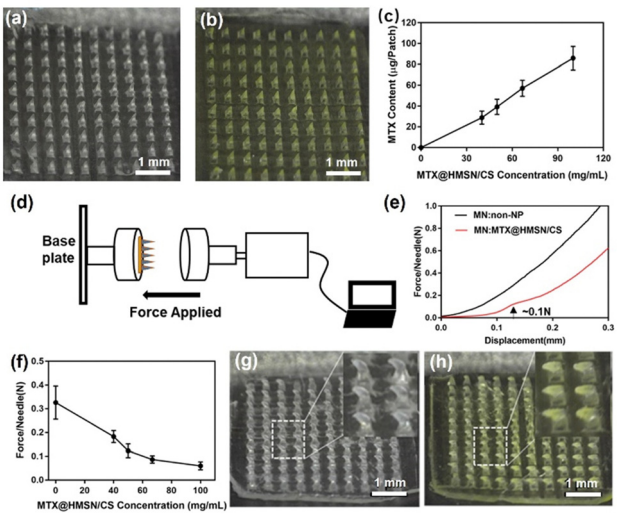

Fig. 4 Morphology, drug loading and mechanical properties of MTX@HMSN/CS-loaded MNs. Representative dermoscope images of (a) unloaded MN patch and (b) MTX@HMSN/CS-loaded MN patch. (c) Relationship between the drug loading of MNs and the concentration of MTX@HMSN/CS. (d) Schematic diagram of the mechanical strength test of the MNs. (e) The force–displacement curves of unloaded MNs and MTX@HMSN/CS-loaded MNs. (f) The analysis of correlation on the drug loading and the mechanical properties of MNs. Dermoscope images of (g) unloaded MNs and (h) MTX@HMSN/CS-loaded MNs bent by the clamp.

3.4. *In vivo* skin insertion experiments of MTX@HMSN/CS-loaded MNs

3.4.1. *In vivo* skin insertion capability and acute skin irritation test of MTX@HMSN/CS-loaded MNs. We investigated the insertion ability of the MNs (the mass ratio of MTX@HMSN/CS to the MN matrix was 1 : 4) using the skin of IMQ-induced psoriasis-like mice. The histological sections of the MN-pierced mouse ear suggested that the MNs could successfully penetrate the psoriasis-like thickened epidermis and effectively deliver MTX@HMSN/CS into the dermis. The penetration depth of the MNs is approximately 180 μm, which is a necessary condition for animal experiments (Fig. 5(a)). In addition, we continuously recorded the recovery process of mouse dorsal skin after MN insertion using a dermoscope (Fig. 5(b)). The puncture marks on the mouse dorsal skin gradually disappeared over time, and the micropore arrays on the skin finally disappeared after 1 h. During the observation, no obvious irritation reaction (erythema or swelling) appeared on the mouse skin. The results indicated that the prepared MNs could penetrate the stratum corneum of skin and directly deliver MTX@HMSN/CSs to the skin lesion. Besides, the skin damage brought by MN treatment is minimal and reversible.

3.4.2. *In vivo* dissolution of MTX@HMSN/CS-loaded MNs. Next, we continued to investigate the dissolution of MNs loaded with MTX@HMSN/CS in the interstitial fluid of the skin. After the MNs were inserted into the mouse skin, the MNs were removed from the mouse skin at different time points (0, 3, 5, and 8 min), and the dissolution of the MNs was observed under an optical microscope (Fig. 5(c)). ChS has excellent water solubility. The sharp tips of the MNs disappeared after 3 minutes of insertion into the skin, and most of the needles dissolved within several minutes after insertion into the skin. The changes in the surface morphology of these drug-loaded

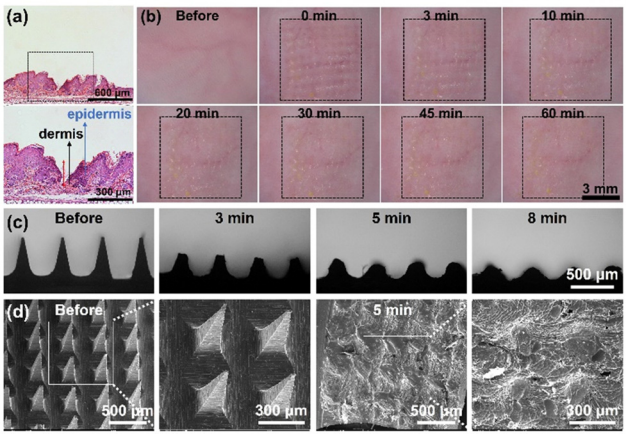

Fig. 5 *In vivo* skin insertion evaluation of MTX@HMSN/CS-loaded MNs. (a) Optical micrographs of H&E staining of skin sections from psoriatic mice after microneedling. (b) Dermoscope images of MN-treated mouse dorsal skin at different time intervals. (c) Optical microscope photos and (d) SEM photos of MTX@HMSN/CS-loaded MNs over time after insertion into the back of mice *in vivo*. The scale bars in the last images can be applied to the other images for the same types.

MN patches were observed under SEM after the MNs were inserted into the mouse skin for 5 minutes (Fig. 5(d)). Before dissolving, the MNs form a relatively regular quadrangular pyramid array structure, and the needle tips are sharp and prominent. After 5 minutes, the needle tips disappear, the substrate of MN patch becomes rough, and the needles become blunt protrusions, suggesting that the drug-loaded MN patch penetrated the mouse skin and contacted the interstitial fluid. The needles prepared with ChS could be rapidly dissolved by the interstitial fluid so that the MTX@HMSN/CS in the needles were released into the skin at the same time.

3.5. Drug permeation study of MTX@HMSN/CS-loaded MNs

To observe drug penetration into the skin, we replaced MTX with R6G during MN preparation. The R6G@HMSN/CS-loaded MN patch pierced into fresh pig skin. And the fluorescent signal in skin was observed using CLSM after 5 minutes. We found that the diffusion depth of the dye R6G in the skin reached about 200 μm, which is less than the length of the needle (Fig. 6). This is largely due to the fact that MN cannot completely penetrate the skin because of the viscoelasticity of the skin. In addition, since the tip of the MN is pyramid-shaped, its cross-sectional area and the amount of dye-loaded HMSN/CS decreased from the base to the tip. Thus, it can also be seen that as the depth of the scanning plane increased, the fluorescence intensity became weaker and weaker. It is worth noting that the insertion depth of MN into the skin is around 200 μm, which avoids the contact of the MN with the nerve fibers and capillaries, significantly reducing the damage and pain, thereby improving patient compliance.

3.6. *In vitro* cell experiments

Then, we employed HaCaT cells to preliminarily evaluate the anti-proliferative effect of MTX@HMSN/CS using CCK-8 assay. IL-1β, IL-6, and CCL20 are important proinflammatory cytokines and chemokines in the pathogenesis of psoriasis, which further exacerbates skin lesion.[40–42] IL-17A accelerates the proliferation and inflammatory response of keratinocytes.[43] Therefore, we determined the concentrations of IL-1β, IL-6, and CCL20 in the supernatants to estimate the anti-inflammatory effects of MTX@HMSN/CS. We stimulated the proliferation of HaCaT cells by adding IL-17A to simulate the inflammatory microenvironment in psoriasis-like skin. HaCaT cells in different groups were incubated at 37 °C with various concentrations of HMSN/CS or MTX@HMSN/CS for 48 hours. After adding a certain amount of IL-17A (100 ng mL^{-1}), HaCaT cells exhibited enhanced proliferation. However, when adding IL-17A and different concentrations of blank HMSN/CS at the same time, the survival rate of HaCaT cells was not significantly different from that of the IL-17A group, indicating that HMSN/CS had no obvious toxicity to HaCaT cells in the concentration range of 0.01 to 10 μg mL^{-1}. In the IL-17A + MTX@HMSN/CS group, we found that when the concentration of MTX was more significant than 0.1 μg mL^{-1}, the survival rate and the secretion levels of IL-1β, IL-6, and CCL20 in HaCaT cells gradually decreased with increasing MTX@HMSN/CS concentration (Fig. 7(a)–(d)). The above results showed that HMSN/CS had good biocompatibility and that MTX@HMSN/CS could effectively suppress epidermal hyperplasia and the expressions of proinflammatory cytokines (IL-1β, IL-6) and chemokines (CCL20).

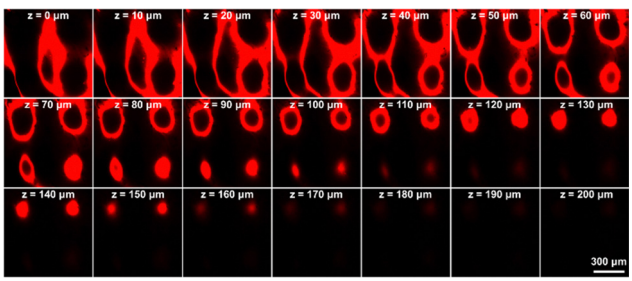

Fig. 6 Drug permeation study of MTX@HMSN/CS-loaded MNs. CLSM images of R6G@HMSN/CS-loaded MNs inserted into pig skin at different depths. The scale bar in the last image applies to the others.

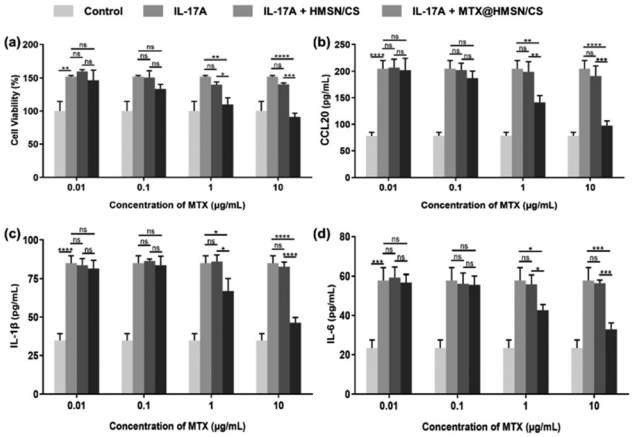

Fig. 7 *In vitro* inhibitory effect of MTX@HMSN/CS loaded in MNs on HaCaT cells. (a) The cell viability and the expression of (b) CCL20, (c) IL-1β, and (d) IL-6 of HaCaT cells after incubation with different concentrations of HMSN/CS or MTX@HMSN/CS for 48 hours. Data are presented as mean ± SD (n = 5) (ns, $p > 0.05$; *, $p < 0.05$; **, $p < 0.01$; ***, $p < 0.001$; ****, $p < 0.0001$).

3.7. *In vivo* transdermal drug delivery study

Finally, we investigated the therapeutic and adverse effects of the MTX@HMSN/CS-loaded MN patch in psoriasis-like mice and compared them with the results of the MTX-loaded MN patch. Fig. 8(a) shows the scheme of the animal experiment. 15.8 μg MTX-loaded MN patch was used to treat psoriasis-like mice once daily to achieve a manual slow-release drug effect. However, the mice in the other groups were treated on day 1, day 4, and day 7. After the mice were sacrificed on day 10, we measured the thickness of the left ears and took pictures of them. In the psoriasis-like mouse model group, the unloaded MN group and the HMSN/CS MN group, the thickness of mice left ear gradually increased to ~550 μm on the 10th day with skin erythema, covered with silvery white scales due to IMQ induction. The final results suggested that the 15.8 μg

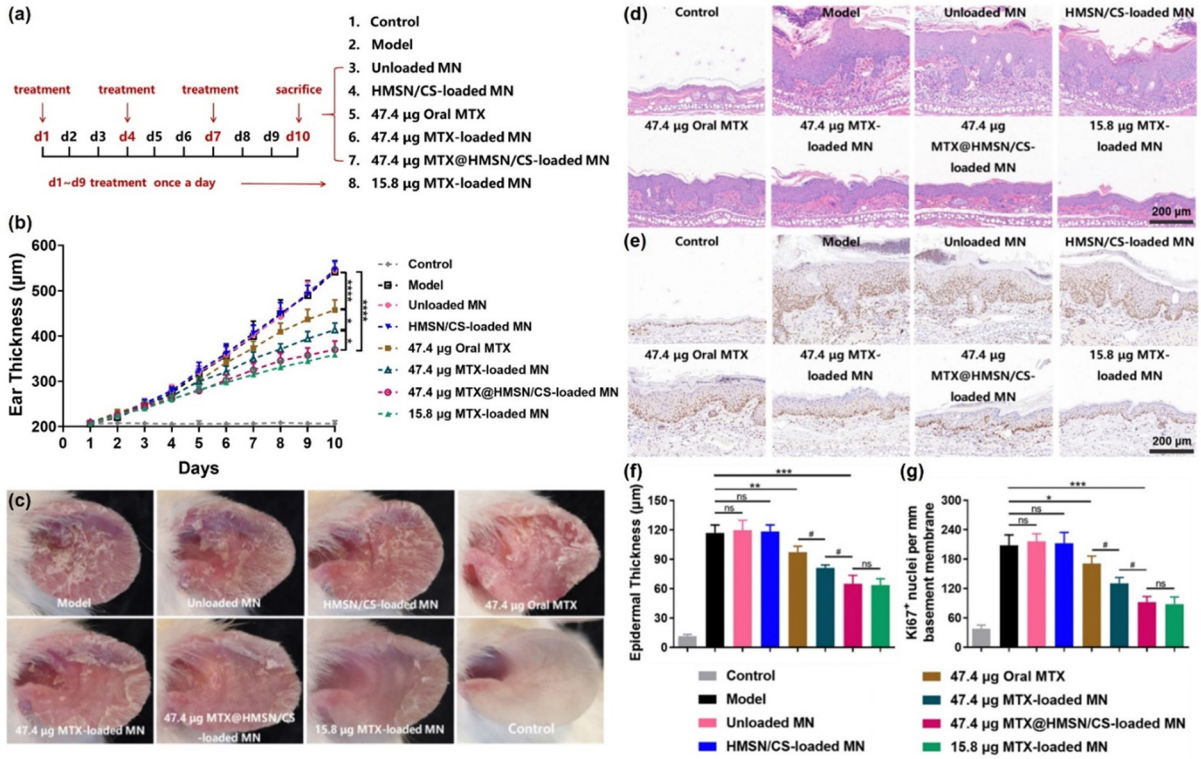

Fig. 8 *In vivo* transdermal drug delivery study of MTX@HMSN/CS-loaded MNs. (a) Timeline of animal experiments. (b) Change curve of left ear thickness of mice under different treatments. (c) Representative photographs of mice left ears in different groups on day 10. Optical microscope photographs of (d) H&E staining and (e) Ki67 immunohistochemical staining of mice left ear skin sections on day 10. The scale bars in the last images can be applied to the other images for the same types. Quantitative analysis of (f) epidermal thickness of mouse left ears and (g) the counts of $Ki67^+$ nuclei per millimeter of basement membrane on day 10. Data are presented as the mean ± SD (n = 5) (ns, $p > 0.05$; *, $p < 0.05$; **, $p < 0.01$; ***, $p < 0.001$; ****, $p < 0.0001$; #, $p < 0.05$).

MTX-loaded MN group and the 47.4 μg MTX@HMSN/CS-loaded MN group showed the best therapeutic effects. The skin scales and erythema of mice in these two groups were much less significant than those in the psoriasis-like mice in the other groups. There was also no significant difference in the thickness of the left ears between these two groups, but the MTX@HMSN/CS-loaded MNs reduced the frequency of MN patch application (once every three days), which was more convenient than daily treatment of 15.8 μg MTX-loaded MN (Fig. 8(b) and (c)).

Previous literature has reported that once the MNs deposit the nanocarriers in the skin, they can effectively accumulate at the site, allowing for a sustained release of the drug from the nanocarriers to maintain the necessary concentration for local therapy.[44–46] Based on previous findings and the results of our study, we initially speculated that after the MTX@HMSN/CS-loaded MNs penetrated the skin and dissolved within several minutes, the MTX@HMSN/CS were quickly released and remained in the skin for an extended period to provide a sustained release of MTX, which improved the availability of the drug and the efficiency of the treatment. The alleviation of psoriasis-like skin inflammation by oral administration of MTX (~47.4 μg) was the weakest, possibly due to the lower drug absorption and utilization rate caused by first-pass elimination. The treatment of 47.4 μg MTX-loaded MN patches was slightly better because the MNs directly delivered the drug into the local skin, avoiding first-pass elimination. However, the MN tips of MTX-loaded MN patches dissolved rapidly after being inserted into the skin. Some drugs were absorbed into skin blood vessels and washed out quickly, reducing the local drug concentration and efficacy. H&E staining and Ki67 immunohistochemical staining were used to further analyze the hyperplasia of the epidermis in psoriasis-like lesions (Fig. 8(d) and (e)). The epidermal thickness of the mouse skin in the model group increased from 11.44 ± 1.74 μm to 117 ± 7.95 μm on day 10 because of IMQ induction. The epidermal thicknesses of the skin lesions in the unloaded MN group and the HMSN/CS-loaded MN group were 119.6 ± 10.24 μm and 118.4 ± 6.67 μm, respectively, indicating no inhibitory effect on epidermal hyperplasia. The epidermal thickness of the left ears of the mice in the oral MTX group, the 47.4 μg MTX-loaded MN group, the 47.4 μg MTX@HMSN/CS-loaded MN group and the 15.8 μg MTX-loaded MN group were reduced to 97.35 ± 5.99 μm, 81.21 ± 2.80 μm, 65.06 ± 8.49 μm and 63.68 ± 6.35 μm, respectively (Fig. 8(f)). In addition, IMQ induced marked upregulation of Ki67 expression and $IL\text{-}17A^+$ T cells in the model group, unloaded MN group and HMSN/CS-loaded MN group. The Ki67 expression level and the number of $IL\text{-}17A^+$ T cells of the mouse ears in the 47.4 μg MTX@HMSN/CS-loaded MN group and the 15.8 μg MTX-loaded MN group were the lowest,

indicating the most effective antiproliferative and anti-inflammatory effects (Fig. 8(g) and Fig. S2, ESI†). These results suggested that the MTX@HMSN/CS-loaded MN patches not only inhibited the epidermal hyperplasia and skin inflammation of psoriasis-like mice more effectively but also reduced the frequency of medications, thus improving the efficiency and convenience of the therapy.

We collected and tested the serum of the mice on day 10 to estimate whether the liver and kidney functions of the mice were affected after the treatments. Alanine aminotransferase (ALT), aspartate aminotransferase (AST), blood urea nitrogen (BUN), and creatinine (CREA) are commonly used indicators of liver and kidney function. None of the indicators changed significantly, and they were all within the normal range, indicating that the liver and kidney functions of the mice were not impaired after treatments, and the use of MN patches in our experiments was highly safe (Fig. S3, ESI†).

4. Conclusions

In summary, we have constructed MTX@HMSN/CS-loaded dissolving MN patches that could continuously release MTX for sustained anti-inflammatory effects in psoriasis therapy. First, MTX was loaded into HMSN, and then CS was adsorbed onto the surface of HMSN through electrostatic interactions to avoid rapid drug release. *In vitro* studies suggested that MTX@HMSN/CSs could release MTX in a sustained manner for at least a week and showed antiproliferative and anti-inflammatory effects on HaCaT cells. Then, the MN patch was prepared by dissolving and dispersing the nanocarriers in the polymer solution of the MN matrix. The MTX@HMSN/CS-loaded MN patch effectively reduced the risks and inconvenience of frequent treatments with a continuous release of MTX, thus improving the bioavailability, therapeutic efficacy, and patient compliance. We used the prepared MN patches to treat psoriasis-like mice, and the results showed that these MN patches loaded with MTX@HMSN/CS were superior to MTX-loaded MNs due to enhanced and sustained anti-inflammatory effects. This strategy of combining drug-loaded NPs with dissolving MNs provides a new idea for improving the clinical application of MTX and a potentially better choice for treating psoriasis in the future.

Conflicts of interest

There are no conflicts to declare.

Acknowledgements

This work was supported by the National Natural Science Foundation of China (82071844, 82130089, 82171789 and 82304022). We also thank the Analytical and Testing Center of Huazhong University of Science and Technology for allowing us to use its facilities.

Notes and references

1 C. E. M. Griffiths, A. W. Armstrong, J. E. Gudjonsson and J. N. W. N. Barker, *Lancet*, 2021, **397**, 1301–1315.
2 U. Mrowietz, J. Barker, C. Conrad, D. Jullien, P. Gisondi, A. Flower, J. Reddy, M. Paris, H. Picard, S. Jardon and M. Augustin, *J. Eur. Acad. Dermatol. Venereol.*, 2023, **37**, 348–355.
3 H. Yen, C. H. Huang, I. H. Huang, W. K. Hung, H. J. Su, H. Yen, C. C. Tai, W. Y. Haw, C. Flohr, Z. Z. N. Yiu and C. C. Chi, *Br. J. Dermatol.*, 2022, **187**, 178–187.
4 A. W. Armstrong and C. Read, *JAMA*, 2020, **323**, 1945–1960.
5 S. Dogra and R. Mahajan, *Clin. Exp. Dermatol.*, 2013, **38**, 573–588.
6 H. Montaudié, E. Sbidian, C. Paul, A. Maza, A. Gallini, S. Aractingi, F. Aubin, H. Bachelez, B. Cribier, P. Joly, D. Jullien, M. Le Maître, L. Misery, M. A. Richard and J. P. Ortonne, *J. Eur. Acad. Dermatol. Venereol.*, 2011, **25**, 12–18.
7 S. B. Kaushik and M. G. Lebwohl, *J. Am. Acad. Dermatol.*, 2019, **80**, 27–40.
8 S. Dogra, N. Singh, S. Kumar, T. Narang and S. Handa, *Dermatol. Ther.*, 2022, **35**, e15656.
9 D. M. W. Balak, S. Gerdes, A. Parodi and L. Salgado-Boquete, *Dermatol. Ther.*, 2020, **10**, 589–613.
10 I. Usach, R. Martinez, T. Festini and J. E. Peris, *Adv. Ther.*, 2019, **36**, 2986–2996.
11 T. Sheng, B. Luo, W. Zhang, X. Ge, J. Yu, Y. Zhang and Z. Gu, *Adv. Drug Delivery Rev.*, 2021, **179**, 113919.
12 K. M. Hamed, I. M. Dighriri, A. F. Baomar, B. T. Alharthy, F. E. Alenazi, G. H. Alali, R. H. Alenazy, N. T. Alhumaidi, D. H. Alhulayfi, Y. B. Alotaibi, S. S. Alhumaidan, Z. A. Alhaddad, A. A. Humadi, S. A. Alzahrani and R. H. Alobaid, *Cureus*, 2022, **14**, e29518.
13 D. Ezhilarasan, *Toxicology*, 2021, **458**, 152840.
14 F. Hu, Q. Gao, J. Liu, W. Chen, C. Zheng, Q. Bai, N. Sun, W. Zhang, Y. Zhang and T. Lu, *J. Mater. Chem. B*, 2023, **11**, 2830–2851.
15 R. Li, L. Zhang, X. Jiang, L. Li, S. Wu, X. Yuan, H. Cheng, X. Jiang and M. Gou, *J. Controlled Release*, 2022, **350**, 933–948.
16 J. Chen, H. Ren, P. Zhou, S. Zheng, B. Du, X. Liu and F. Xiao, *Front. Bioeng. Biotechnol.*, 2022, **10**, 1032041.
17 F. Sabbagh and B. S. Kim, *J. Controlled Release*, 2022, **341**, 132–146.
18 B. Z. Chen, Z. Q. Zhao, M. A. Shahbazi and X. D. Guo, *Nanoscale Horiz.*, 2022, **7**, 715–728.
19 Q. Chen, Z. Xiao, C. Wang, G. Chen, Y. Zhang, X. Zhang, X. Han, J. Wang, X. Ye, M. R. Prausnitz, S. Li and Z. Gu, *ACS Nano*, 2022, **16**, 18223–18231.
20 S. Ray, D. M. Wirth, O. A. Ortega-Rivera, N. F. Steinmetz and J. K. Pokorski, *Biomacromolecules*, 2022, **23**, 903–912.
21 T. Sheng, B. Luo, W. Zhang, X. Ge, J. Yu, Y. Zhang and Z. Gu, *Adv. Drug Delivery Rev.*, 2021, **179**, 113919.
22 L. Yang, Y. Yang, H. Chen, L. Mei and X. Zeng, *Asian J. Pharm. Sci.*, 2022, **17**, 70–86.

23 T. Waghule, G. Singhvi, S. K. Dubey, M. M. Pandey, G. Gupta, M. Singh and K. Dua, *Biomed. Pharmacother.*, 2019, **109**, 1249–1258.
24 R. Donnelly, E. Caffarel-Salvador, H. Gill and H. Jung, *J. Mater. Chem. B*, 2023, **11**, 9323–9324.
25 N. G. Rouphael, M. Paine, R. Mosley, S. Henry, D. V. McAllister, H. Kalluri, W. Pewin, P. M. Frew, T. Yu, N. J. Thornburg, S. Kabbani, L. Lai, E. V. Vassilieva, I. Skountzou, R. W. Compans, M. J. Mulligan, M. R. Prausnitz and TIV-MNP 2015 Study Group, *Lancet*, 2017, **390**, 649–658.
26 D. Yang, M. Chen, Y. Sun, Y. Jin, C. Lu, X. Pan, G. Quan and C. Wu, *Acta Biomater.*, 2021, **121**, 119–133.
27 Z. Sartawi, C. Blackshields and W. Faisal, *J. Controlled Release*, 2022, **348**, 186–205.
28 M. Jang, B. M. Kang, H. Yang, J. Ohn, O. Kwon and H. Jung, *Adv. Healthcare Mater.*, 2021, **10**, 2001691.
29 J. Ohn, M. Jang, B. M. Kang, H. Yang, J. T. Hong, K. H. Kim, O. Kwon and H. Jung, *Adv. Sci.*, 2021, **8**, 2004873.
30 H. Du, P. Liu, J. Zhu, J. Lan, Y. Li, L. Zhang, J. Zhu and J. Tao, *ACS Appl. Mater. Interfaces*, 2019, **11**, 43588–43598.
31 R. Chang, L. Chen, M. Qamar, Y. Wen, L. Li, J. Zhang, X. Li, E. Assadpour, T. Esatbeyoglu, M. S. Kharazmi, Y. Li and S. M. Jafari, *Adv. Colloid Interface Sci.*, 2023, **318**, 102933.
32 Y. Eygeris, M. Gupta, J. Kim and G. Sahay, *Acc. Chem. Res.*, 2022, **55**, 2–12.
33 S. Haddadzadegan, F. Dorkoosh and A. Bernkop-Schnürch, *Adv. Drug Delivery Rev.*, 2022, **182**, 114097.
34 F. Qu, R. Geng, Y. Liu and J. Zhu, *Theranostics*, 2022, **12**, 3372–3406.
35 W. Zhu, J. Mei, X. Zhang, J. Zhou, D. Xu, Z. Su, S. Fang, J. Wang, X. Zhang and C. Zhu, *Adv. Mater.*, 2022, **34**, e2207961.
36 S. Hu, D. Zhu, Z. Li and K. Cheng, *ACS Nano*, 2022, **16**, 15935–15945.
37 I. A. Tekko, A. D. Permana, L. Vora, T. Hatahet, H. O. McCarthy and R. F. Donnelly, *Eur. J. Pharm. Sci.*, 2020, **152**, 105469.
38 H. Wang, Z. Zhao, C. Wu, X. Tong, Y. Shi and S. Chen, *Int. J. Nanomed.*, 2022, **17**, 3841–3851.
39 Q. Liu, N. Xu, L. Liu, J. Li, Y. Zhang, C. Shen, K. Shezad, L. Zhang, J. Zhu and J. Tao, *ACS Appl. Mater. Interfaces*, 2017, **9**, 21673–21687.
40 H. T. Meitei, N. Jadhav and G. Lal, *Autoimmun. Rev.*, 2021, **20**, 102846.
41 C. Schinocca, C. Rizzo, S. Fasano, G. Grasso, L. La Barbera, F. Ciccia and G. Guggino, *Front. Immunol.*, 2021, **12**, 637829.
42 L. Tang and F. Zhou, *Front. Immunol.*, 2020, **11**, 882.
43 M. Furue, K. Furue, G. Tsuji and T. Nakahara, *Int. J. Mol. Sci.*, 2020, **21**, 1275.
44 L. K. Vora, R. F. Donnelly, E. Larrañeta, P. González-Vázquez, R. R. S. Thakur and P. R. Vavia, *J. Controlled Release*, 2017, **265**, 93–101.
45 W. Zhang, J. Gao, Q. Zhu, M. Zhang, X. Ding, X. Wang, X. Hou, W. Fan, B. Ding, X. Wu, X. Wang and S. Gao, *Int. J. Pharm.*, 2010, **402**, 205–212.
46 J. Tu, G. Du, M. Reza Nejadnik, J. Mönkäre, K. van der Maaden, P. H. H. Bomans, N. A. J. M. Sommerdijk, B. Slütter, W. Jiskoot, J. A. Bouwstra and A. Kros, *Pharm. Res.*, 2017, **34**, 1693–1706.